Articles

Theoretical and Structural Analysis of the Unsymmetrical Bridging Coordination Mode of the Nonconical PNR_2 Ligands in $Ru_4(CO)_{12}(\mu_4\text{-}PNR_2)_2$ Clusters

Samia Kahlal,[†] Konstantin A. Udachin,[§] Ludmila Scoles,[§] Arthur J. Carty,*[,§] and Jean-Yves Saillard*[,†]

LCSIM UMR-CNRS 6511, Université de Rennes 1, 35042 Rennes Cedex, France, and Steacie Institute for Molecular Sciences, NRC, 100 Sussex Drive, Ottawa, Canada K1A OR6

Received December 28, 1999

The X-ray molecular structure of $Ru_4(CO)_{12}(\mu_4\text{-}PNEt_2)_2$ exhibits a strong distortion of its octahedral Ru_4P_2 core toward D_{2d} symmetry, with a puckered Ru_4 "square" and a phosphorus coordination mode intermediate between μ_4 and μ_2. The electronic origin of this distortion is analyzed with the help of EHT and DFT calculations. This structural peculiarity originates from the nonconical nature of the PNR_2 ligand and from the ability of the $Ru_4(CO)_{12}$ unit to adapt its conformation and bonding ability to this unsymmetrical bonding.

Introduction

Transition-metal clusters exhibiting an $M_4(\mu_4\text{-}E)_2$ octahedral core of pseudo-D_{4h} symmetry (**1**) in which a

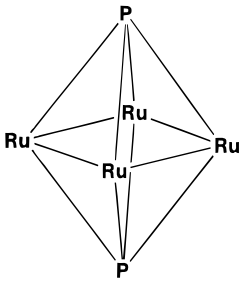

1

metallic M_4 square is capped on both sides by a main-group E ligand are well documented.[1,2] An interesting feature of this type of cluster is that they can possess two different closed-shell electron counts, depending on the nature of the metal atoms. One possible electron count is 62 metal valence electrons (MVEs), which corresponds to seven skeletal electron pairs (SEP) in the electron-counting framework of polyhedral electron pair theory (PSEPT).[3] The other electron count is 64 MVEs, which corresponds to eight SEPs. With 62 MVEs, the metal centers are electron-deficient with respect to the 18-electron rule, but being a 7-SEP closo M_4E_2 octahedra, they obey the PSEPT electron-counting rules. On the other hand, the 64-MVE count allows the metal atoms to reach the 18-electron count, but the cluster is electron-rich with respect to the PSEPT rules. In our previous work on the electronic structure and bonding of these octahedral systems and related M_4E_2 species we have shown that the existence of these two closed-shell electron counts is related to the position of a molecular orbital (MO) of b_{1u} pseudosymmetry, which lies approximately in the middle of a large energy gap separating the bonding levels from the antibonding ones, as schematized in Figure 1. Thus, the closed-shell requirement is secured by a significant HOMO/LUMO gap, whether the b_{1u} level is the LUMO (62 MVEs) or the HOMO (64 MVEs). The intermediate energy position of this level is due to two factors: (i) the approximate D_{4h} symmetry of the cluster core, which does not allow E mixing into the LUMO; (ii) its weak M−M antibonding character, which is intermediate between π^* and δ^* (Figure 1). Calculations have shown that the position of the b_{1u} orbital in the energy gap strongly depends on the energy of the constituent metallic AOs.[1] Therefore electronegative metals favor $\Delta_1 < \Delta_2$, while electropositive metals favor $\Delta_2 < \Delta_1$. The lower the energy of the b_{1u} level, the more favored the 64 MVE count and conversely. To date there have been no experimentally observed exceptions to this trend. Indeed, all of the characterized octahedral Co_4E_2 clusters contain 64 MVEs (8 SEPs), while all of the octahedral Ru_4E_2 clusters contain 62 MVEs (7 SEPs). Iron clusters have been characterized with either 64 MVEs or 62

[†] LCSIM UMR-CNRS 6511, Université de Rennes 1.
[§] Steacie Institute for Molecular Sciences.

(1) (a) Halet, J.-F.; Hoffmann, R.; Saillard, J.-Y. *Inorg. Chem.* **1985**, *25*, 1695. (b) Halet, J.-F.; Saillard, J.-Y. *New J. Chem.* **1987**, *11*, 315.
(2) Halet, J.-F. *Coord. Chem. Rev.* **1995**, *143*, 637.
(3) See for example: (a) Wade, K. In *Transition Metal Clusters*; Jonhson, B. F. G., Ed.; Wiley and Sons: New York, 1980; p 193. (b) Mingos, D. M. P.; Wales, D. J. *Introduction to Cluster Chemistry*; Prentice-Hall: Englewood Cliffs, NJ, 1990.

10.1021/om991038r CCC: $19.00
Publication on Web 05/16/2000

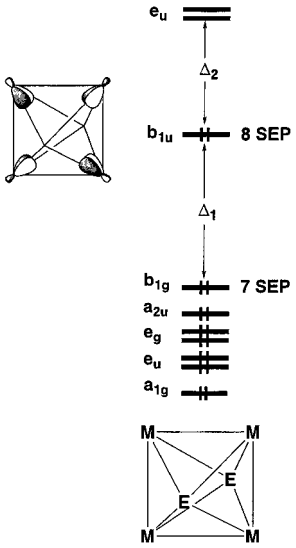

Figure 1. Qualitative MO diagram of a $M_4L_n(\mu_4\text{-}E)_2$ cluster exhibiting an M_4E_2 core of pseudo-D_{4h} symmetry.

MVEs, in agreement with the electronegativity of this metal, which is intermediate between those of Co and Ru.

In this context, the recent synthesis and structural characterization by Carty and co-workers of a 64-MVE ruthenium species, $Ru_4(CO)_{12}(\mu_4\text{-}PNR_2)_2$ ($R = Pr^i$),[4] and the confirmation in this paper that $Ru_4(CO)_{12}(\mu_4\text{-}PNR_2)_2$ ($R = Et$) has the same geometry is somewhat surprising. For such a Ru_4E_2 skeleton, our previous theoretical investigations predict the octahedral arrangement to be unstable with respect to the opening of one of its edges, leading to a *nido*-type structure in agreement with the PSEP theory.[2] Moreover, the $Ru_4(CO)_{12}(\mu_4\text{-}PNR_2)_2$ clusters present a pronounced core distortion away from the ideal D_{4h} symmetry, but different from the nido-type open octahedron expected for this electron count. This distortion, schematized in **2**, leads to a Ru_4P_2 skeleton

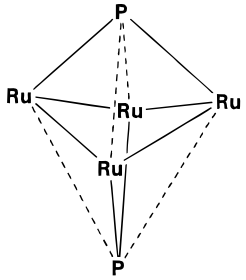

2

of pseudo-D_{2d} symmetry. The Ru_4 "square" is puckered away from planarity, with a butterfly bending angle of 135° and 137° for $R = Pr^i$ and Et, respectively. The phosphorus coordination mode is intermediate between μ_4 and μ_2 with two short P−Ru separations (average = 2.28 and 2.27 Å for $R = Pr^i$ and Et, respectively) and two long ones (average 2.78 and 2.74 Å for $R = Pr^i$ and Et, respectively). The PNR_2 ligands are planar and the PN distance is intermediate between standard values for single and double bonds (average 1.67 and 1.66 Å for $R = Pr^i$ and Et, respectively).[4]

(4) Wang, W.; Corrigan, J. F.; Enright, G. D.; Taylor, N. J.; Carty, A. J. *Organometallics* **1998**, *17*, 427.

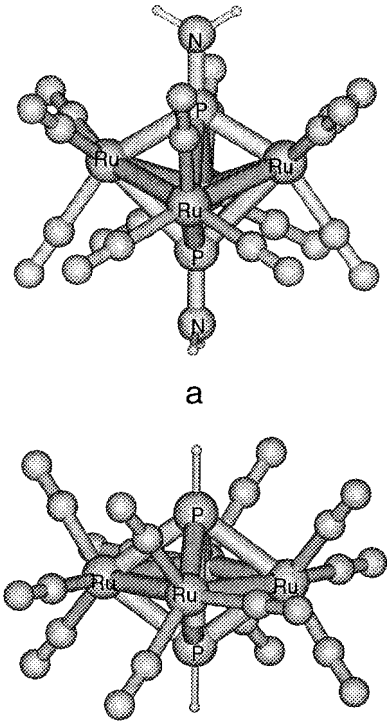

a

b

Figure 2. Idealized geometries of the $Ru_4(CO)_{12}(\mu_4\text{-}PNH_2)_2$ model assuming D_{2d} symmetry (a) and of the $Ru_4(CO)_{12}(\mu_4\text{-}PH)_2$ model assuming C_{4h} symmetry (b).

Another structural peculiarity of the $Ru_4(CO)_{12}(\mu_4\text{-}PNR_2)_2$ compounds is that the CO ligands are in a peculiar positional orientation as compared to classical $M_4L_n(\mu_4\text{-}E)_2$ phosphinidene species.[2] In the case of $Ru_4(CO)_{12}(\mu_4\text{-}PNR_2)_2$, the CO ligands are placed in such a way that they are approximately trans to the short Ru−P bonds so that, if one does not consider the Ru−Ru and the long P−Ru bonds, the metal atoms lie in a distorted trigonal bipyramidal environment. This confers to the whole $Ru_4(CO)_{12}(\mu_4\text{-}PNR_2)_2$ molecule an ideal D_{2d} symmetry, shown in Figure 2a. In this peculiar ligand orientation where no ligand lies in the "horizontal" plane, the up and down sides of each Ru atom are inequivalent, even assuming a planar Ru_4 arrangement. This inequivalence is not present in most of the classical $M_4L_n(\mu_4\text{-}E)_2$ clusters.[2] In the case of a $Ru_4(CO)_{12}(\mu_4\text{-}PR)_2$ species, the inequivalence can be removed by orientating the CO ligands in such a way that the ideal molecular symmetry is C_{4h}, with four "in-plane" carbonyls (Figure 2b).

Assuming the regular arrangement **1** for the Ru_4P_2 core of $Ru_4(CO)_{12}(\mu_4\text{-}PNR_2)_2$, the Δ_2 HOMO/LUMO gap is expected to be rather small (see above), suggesting second-order Jahn−Teller instability. However, none of the lowest vacant levels has the required symmetry to allow a mixing with the HOMO which would lead to the D_{2d} distortion **2**. It turns out that this distortion is in fact related to the nonconical bonding ability of the peculiar PNR_2 ligands, as shown by our theoretical investigations described below. Calculations have been carried out at two levels of theory. A detailed orbital analysis has been at first provided through a series of extended Hückel theory (EHT) calculations with the help of a computer package that allows a deep insight

Table 1. Crystal Data and Structure Refinement for $[Ru_4(CO)_{12}(\mu_4\text{-}PNEt_2)_2]$

empirical formula	$C_{20}H_{20}N_2O_{12}P_2Ru_4$
fw	946.60
temperature (K)	173(2)
wavelength (Å)	0.71070
cryst syst	monoclinic
space group	$P2_1/c$
a (Å)	9.380(2)
b (Å)	16.917(3)
c (Å)	19.244(3)
α (deg)	90.
β (deg)	94.737(3)
γ (deg)	90
V, Å^3	3043.4(9)
Z	4
D_{calc}, g cm^{-3}	2.066
abs coeff mm^{-1}	2.110
F(000)	1824
cryst size, mm	0.2 × 0.3 × 0.3
θ range for data collection (deg)	1.61−28.82
index ranges	$-12 \le h \le 11$, $-22 \le k \le 22$, $-25 \le l \le 26$
no. of reflns collected/unique	30903/7892 [R(int) = 0.0568]
completeness to $2\theta = 28.82$	96.1%
refinement method	full-matrix least-squares on F^2
data/restraints/params	7892/0/361
goodness-of-fit on F^2	1.033
final R indices [$I > 2\sigma(I)$]	R1 = 0.0272, wR2 = 0.0616
R indices (all data)	R1 = 0.0387, wR2 = 0.0655
largest diff peak and hole	0.971 and −0.811 e Å^{-3}

into the orbital interaction between atoms or fragments. To confirm the qualitative EHT conclusions and to complete them with more quantitative results, selected density functional theory (DFT) calculations, which allow geometry optimization, were carried out in a second step.

Experimental Section

Synthesis of $Ru_4(CO)_{12}(\mu_4\text{-}PNEt_2)_2$. A Schlenk tube was charged with $Ru_3(CO)_{12}$ (622 mg, 0.64 mmol), benzophenone (533 mg, 1.4 mmol), potassium metal (114 mg, 1.4 mmol), and dry, degassed THF (12 mL). After stirring at room temperature for 2 h under nitrogen the reaction mixture was warmed to 55−60 °C and stirred for a further 46 h. The resulting $K_4[Ru_4(CO)_{12}]$ was not isolated but treated with Cl_2PNEt_2 (210 μL, 1.4 mmol), and the deep red solution was stirred for 2 h. The solvent was removed in vacuo, and the oily residue redissolved in CH_2Cl_2 and adsorbed onto silica gel. Column chromatography (hexane eluant), followed by extraction of the crude product with hexane to remove residual $Ru_3(CO)_{12}$ and recrystallization from CH_2Cl_2/MeOH (4−5 days at −28 °C) gave dark orange, air-stable crystals of $Ru_4(CO)_{12}(\mu_4\text{-}PNEt_2)_2$ (130 mg, 21%).

Spectral Data. IR (CH_2Cl_2): ν(CO), 2061 w, 2042 vs, 2002 m, 1969 w cm^{-1}. ^{1}H NMR (δ, $CDCl_3$): 1.4 (t, $J_{H-H} = 7$ Hz, CH_3), 4.01 (dq, $J_{H-H} = 7$ Hz, $J_{H-P} = 14.0$ Hz, CH_2). $^{31}P\{^1H\}$ (δ, $CDCl_3$): 424.8 s. Anal. Calcd for $Ru_4P_2N_2O_{12}C_{20}H_{20}$: C, 25.27; H, 2.12; N, 2.95. Found: C, 25.59; H, 2.16; N, 2.32.

X-ray Analysis. A red monoclinic single crystal of $Ru_4(CO)_{12}(\mu_4\text{-}PNEt_2)_2$ was mounted on a glass fiber with 5 min. epoxy. X-ray intensity data were collected on a Siemens SMART CCD diffractometer using Mo Kα radiation. Details of data collection, reduction, and refinement are given in Table 1. Atomic coordinates are listed in Table 2, and a summary of important bond lengths and angles is shown in Table 3.

Computational Details

EHT calculations[5] were carried out using the Computed Aided Composition of Atomic Orbitals (CACAO) package.[6] The weighted H_{ij} formula was considered.[7] The atomic parameters used for H, N, C, and O are the standard ones.[5] The P and Ru valence ns and np exponents (ξ) and valence shell ionization potentials (H_{ii} in eV) are given below. 3s(P): 1.600, −18.60; 3p(P): 1.600, −12.40; 5s(Ru): 2.078, −8.6; 5p(Ru) 2.043, −5.1. The Ru 4d valence orbitals ($H_{ii} = -12.20$ eV) were described by a linear combination of two Slater-type orbitals of exponents $\xi_1 = 5.538$ and $\xi_2 = 2.303$ with the weighting coefficients $C_1 = 0.534$ and $C_2 = 0.637$. In the calculated models the following bond distances (Å) and bond angles (deg), based on the average molecular structure of $Ru_4(CO)_{12}(\mu_4\text{-}PNPr^i_2)$,[4] were assumed: Ru−Ru = 2.868; Ru−P = 2.275 and 2.775 (structure **2**); Ru−P = 2.525 (structure **1**); Ru−CO = 1.930; P−N = 1.671, N−H = 1.010; C−O = 1.136; (CO)Ru(CO) = 95.0; HNH = 120.0.

DFT calculations[8] were carried out using the Amsterdam Density Functional (ADF) program.[9] Electron correlation was treated within the local density approximation in the Vosko−Nusair parametrization (LDA).[10] The numerical integration

Table 2. Atomic Coordinates (× 10^4) and Equivalent Isotropic Displacement Parameters (Å^2 × 10^3) for $[Ru_4(CO)_{12}(\mu_4\text{-}PNEt_2)_2]$

atom	x	y	z	U(eq)
Ru(1)	3151(1)	7133(1)	2530(1)	27(1)
Ru(2)	463(1)	6302(1)	2366(1)	27(1)
Ru(3)	2107(1)	4900(1)	2696(1)	27(1)
Ru(4)	4381(1)	5693(1)	2063(1)	30(1)
P(1)	2884(1)	6039(1)	3205(1)	26(1)
P(2)	2175(1)	6083(1)	1616(1)	28(1)
O(9)	6238(3)	7560(2)	2999(1)	54(1)
O(10)	2939(3)	8137(2)	1179(1)	63(1)
O(11)	1683(3)	8328(2)	3418(2)	63(1)
O(12)	783(3)	6579(2)	3793(1)	63(1)
O(13)	1764(2)	5112(1)	1800(1)	45(1)
O(14)	1020(3)	7759(2)	1723(2)	66(1)
O(15)	326(3)	4387(2)	3548(2)	57(1)
O(16)	4214(3)	3714(2)	3376(2)	63(1)
O(17)	1252(3)	3902(2)	1370(1)	60(1)
O(18)	6644(3)	5343(2)	3294(1)	63(1)
O(19)	4877(3)	4149(2)	1312(2)	64(1)
O(20)	6286(3)	6683(2)	1195(1)	59(1)
N(1)	3321(3)	6091(2)	4057(1)	37(1)
N(2)	1768(3)	6164(2)	764(1)	43(1)
C(1)	3892(4)	6808(2)	4414(2)	49(1)
C(2)	5460(5)	6752(3)	4664(2)	73(1)
C(3)	3133(4)	5412(2)	4525(2)	47(1)
C(4)	1803(5)	5458(3)	4907(2)	65(1)
C(5)	2823(4)	5994(3)	254(2)	54(1)
C(6)	2620(6)	5194(3)	84(2)	81(2)
C(7)	339(4)	6353(3)	446(2)	55(1)
C(8)	196(5)	7180(3)	146(2)	74(1)
C(9)	5087(3)	7409(2)	2822(2)	37(1)
C(10)	3015(3)	7774(2)	1673(2)	38(1)
C(11)	2215(4)	7889(2)	3074(2)	40(1)
C(12)	305(3)	6476(2)	3280(2)	38(1)
C(13)	939(3)	5559(2)	2023(2)	32(1)
C(14)	446(4)	7222(2)	1959(2)	41(1)
C(15)	588(4)	4577(2)	3231(2)	39(1)
C(16)	3433(4)	4156(2)	3105(2)	40(1)
C(17)	1532(3)	4263(2)	1857(2)	37(1)
C(18)	5833(3)	5483(2)	2842(2)	41(1)
C(19)	4685(4)	4720(2)	1597(2)	42(1)
C(20)	5579(3)	6319(2)	1519(2)	39(1)

[a] U(eq) is defined as one-third of the trace of the orthogonalized U_{ij} tensor.

(5) Hoffmann, R. *J. Chem. Phys.* **1963**, *39*, 1397.
(6) Mealli, C.; Proserpio, D. *J. Chem. Educ.* **1990**, *67*, 399.
(7) Ammeter, J. H.; Bürgi, H.-B.; Thibeault, J. C.; Hoffmann, R. *J. Am. Chem. Soc.* **1978**, *100*, 3686.
(8) (a) Baerends, E. J.; Ellis, D. E.; Ros, P. *Chem. Phys.* **1975**, *8*, 41. (b) Baerends, E. J.; Ros, P. *Int. J. Quantum Chem.* **1978**, *S12*, 169. (c) Boerrigter, P. M.; te Velde, G.; Baerends, E. J. *Int. J. Quantum Chem.* **1988**, *33*, 87. (d) te Velde, G.; Baerends, E. J. *J. Comput. Phys.* **1992**, *99*, 84.
(9) *Amsterdam Density Functional (ADF) program, version 2.3*; Vrije Universiteit, Amsterdam: Netherlands, 1997.
(10) Vosko, S. D.; Wilk, L.; Nusair, M. *Can. J. Chem.* **1990**, *58*, 1200.

Table 3. Summary of Important Bond Lengths (Å) and Angles (deg) for $[Ru_4(CO)_{12}(\mu_4\text{-}PNEt_2)_2]$

Ru(1)−P(1)	2.2852(8)
Ru(1)−P(2)	2.6117(8)
Ru(2)−P(1)	2.7118(8)
Ru(2)−P(2)	2.2755(8)
Ru(3)−P(1)	2.2557(8)
Ru(3)−P(2)	2.8890(8)
Ru(4)−P(1)	2.7668(8)
Ru(4)−P(2)	2.2715(8)
Ru(1)−Ru(2)	2.8808(5)
Ru(1)−Ru(4)	2.8711(5)
Ru(2)−Ru(3)	2.8712(5)
Ru(3)−Ru(4)	2.8749(5)
P(1)−N(1)	1.660(2)
P(2)−N(2)	1.659(3)
N(1)−C(1)	1.471(4)
N(1)−C(3)	1.479(4)
N(2)−C(5)	1.478(5)
N(2)−C(7)	1.461(5)
P(1)−Ru(1)−P(2)	77.48(3)
P(1)−Ru(3)−P(2)	72.23(3)
P(2)−Ru(2)−P(1)	75.57(3)
P(2)−Ru(4)−P(1)	74.50(3)
Ru(1)−Ru(2)−Ru(4)	47.121(11)
Ru(1)−Ru(4)−Ru(2)	47.331(7)
Ru(1)−Ru(4)−Ru(3)	86.081(14)
Ru(2)−Ru(1)−Ru(3)	46.914(7)
Ru(2)−Ru(3)−Ru(1)	47.119(11)
Ru(2)−Ru(3)−Ru(4)	85.655(14)
Ru(3)−Ru(2)−Ru(4)	47.212(7)
Ru(3)−Ru(4)−Ru(2)	47.134(10)
Ru(4)−Ru(1)−Ru(2)	85.548(14)
Ru(4)−Ru(1)−Ru(3)	47.000(11)
Ru(4)−Ru(3)−Ru(1)	46.919(7)
Ru(1)−P(1)−Ru(2)	69.81(2)
Ru(1)−P(1)−Ru(4)	68.50(2)
Ru(2)−P(1)−Ru(4)	90.95(2)
Ru(3)−P(1)−Ru(1)	119.45(3)
Ru(3)−P(1)−Ru(2)	69.93(2)
Ru(3)−P(1)−Ru(4)	68.97(2)
Ru(1)−P(2)−Ru(3)	90.81(3)
Ru(2)−P(2)−Ru(1)	71.86(2)
Ru(2)−P(2)−Ru(3)	66.32(2)
Ru(4)−P(2)−Ru(1)	71.64(2)
Ru(4)−P(2)−Ru(2)	118.42(3)
Ru(4)−P(2)−Ru(3)	66.46(2)
C(1)−N(1)−C(3)	114.4(3)
C(7)−N(2)−C(5)	114.0(3)

procedure applied for the calculations was developed by te Velde et al. [8d] A triple-ζ Slater-type orbital (STO) basis set was used for Ru 4d and 5s augmented with a single ζ 5p polarization function. A double-ζ STO basis set was employed for H 1s, C, N, and O 2s and 2p, P 3s and 3p, extended with a single-ζ polarization function 2p for H and 3d C, N, O, and P. A frozen-core approximation was used to treat the core electrons of C, O, N, P, and Ru.[8a]

Results and Discussion

X-ray Molecular Structure of $Ru_4(CO)_{12}(\mu\text{-}PNEt_2)_2$. The reaction of the $[Ru_4(CO)_{12}]^{4-}$ anion with two molecules of Cl_2PNEt_2 affords $Ru_4(CO)_{12}(\mu\text{-}PNEt_2)_2$ in moderate yields. The principal structural features of this molecule (Figure 3) are similar to those of $Ru_4(CO)_{12}(\mu_4\text{-}PNPr^i_2)_2$, confirming that the Ru_4P_2 pseudo-D_{2d} symmetry of the latter is not an artifact of the bulky diisopropylamino groups on the phosphinidene ligands. The four Ru−Ru bond lengths in the cluster range from 2.8711(5) to 2.8808(5) Å (av 2.874 Å) and are in the normal range for ruthenium clusters.[4] The Ru_4 framework is a severely distorted square with a dihedral angle of 136.6° between the Ru(1), Ru(2)−Ru(3) and Ru(4),

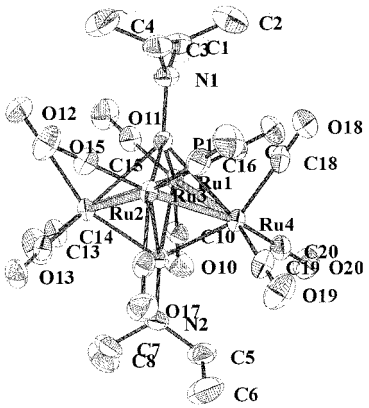

Figure 3. Crystal structure of $Ru_4(CO)_{12}(\mu_4\text{-}PNEt_2)_2$.

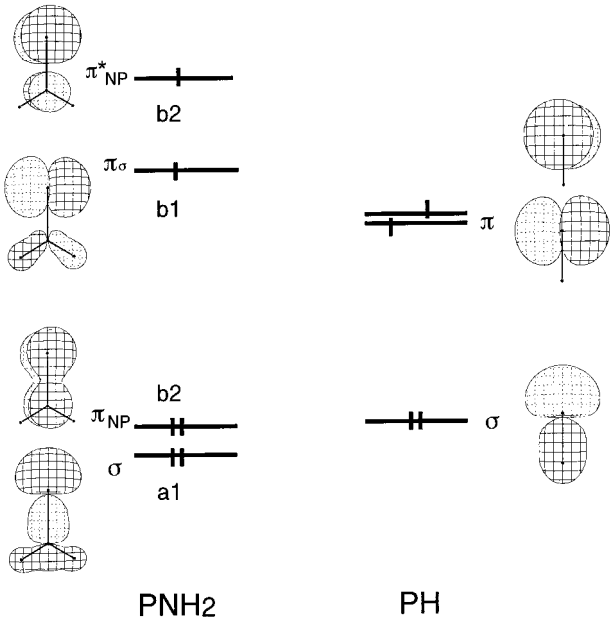

Figure 4. Frontier orbitals of the PNH_2 and PH ligands.

Ru(1), Ru(3) triangles. This distortion toward a D_{2d} butterfly from a D_{4h} square results in two distinct sets of ruthenium−phosphorus bond lengths to each phosphinidene ligand with the shorter bonds P(1)−Ru(1) 2.2852(8) Å, P(1)−Ru(3) 2.2557(8) Å, P(2)−Ru(2) 2.2755(8) Å, and P(2)−Ru(4) 2.2715(8) Å being on average almost 0.5 Å less than the long Ru−P vectors (P(1)−Ru(2) 2.7118(8) Å, P(1)−Ru(4) 2.7668(8) Å, P(2)−Ru(3) 2.8890(8) Å, P(2)−Ru(1) 2.6117(8) Å). In view of these very long Ru−P distances it is tempting to suggest that the interactions are at best only weakly bonding. The P−N bond distances (P(1)−N(1) 1.660(2) Å, P(2)−N(2) 1.659(3) Å) are comparable with values in other aminophosphinidene clusters (range 1.636−1.685 Å) and consistent with partial P−N multiple bonding. Each nitrogen atom has a planar sp^2 coordination environment with C−N−C angles of 114.4(3)° at N(1) and 114.0(3)° at N(2). Clearly, the two compounds $Ru_4(CO)_{12}(\mu_4\text{-}PNR_2)_2$ (R = Et; Pr^i) constitute a novel structural type of the 64-MVE M_4E_2 clusters.

EHT Investigation.A conical fragment, such as a regular P−R alkyl phosphinidene for instance, possesses one σ-type frontier orbital and two π-type frontier orbitals that are degenerate and have exactly the same shape, except that they lie in two different perpendicular planes. This is exemplified on the right side of Figure 4

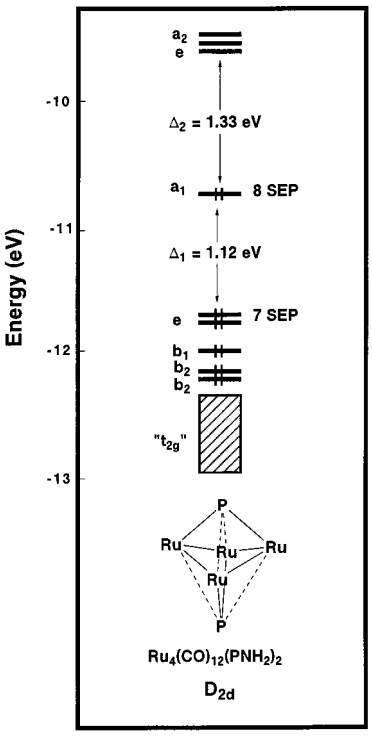

Figure 5. EHT MO level ordering $Ru_4(CO)_{12}(\mu_4\text{-}PH)_2$ calculated assuming the D_{2d} averaged idealized geometry of $Ru_4(CO)_{12}(\mu_4\text{-}PNPr^i)_2$.

by the frontier orbital diagram of a P−H ligand. On the other hand, a planar PNR_2 ligand has two π-type orbitals that have different energies and shapes, as illustrated on the left side of Figure 4 by the frontier orbitals of PNH_2. One of them, labeled π_σ, is essentially a nonbonding $3p_\sigma$ AO, with some antibonding nitrogen admixture. The other one, labeled π^*, can be identified as being the moderately antibonding π^*_{NP} orbital. It has a dominant P localization. EHT calculations indicate that the bonding π_{NP} combination, lying at lower energy, plays a minor role in the bonding and can be discarded in this analysis. From the point of view of frontier orbitals and bonding ability, there is a clear relationship between a planar PNR_2 ligand with diazene or diazenido $(NNR_2)^{0/2-}$ ligands.[11]

Being of different energies and localizations, the two π-type frontier orbitals of PNR_2 have different bonding abilities. This is shown by calculations on the $Ru_4(CO)_{12}(\mu_4\text{-}PNH_2)_2$ model, assuming first of all the Ru_4P_2 core arrangement **1** and the same carbonyl conformation as in Figure 2b. Therefore, in this structural model the $Ru_4(CO)_{12}$ fragment has local C_{4h} symmetry and "sees" equivalently all the Ru−P bonds which are set equal. Despite that, two different Ru−P overlap populations (0.381 and 0.366) are computed in this model of overall C_2 symmetry, the largest value corresponding to the Ru−P bonds lying in the PNR_2 plane. Clearly, this

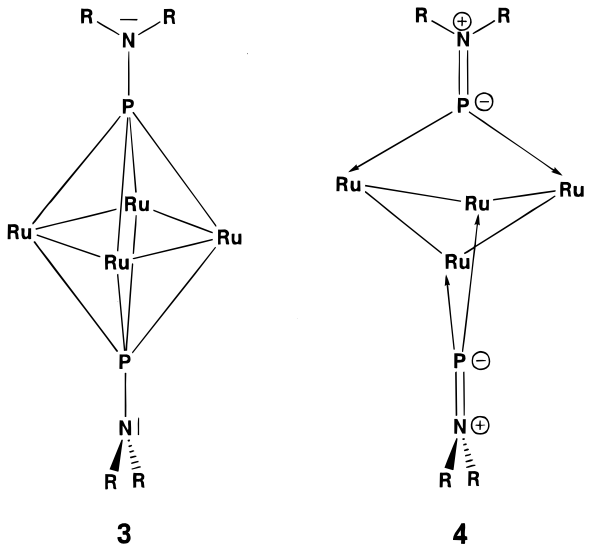

difference is induced by the nonconical nature of the PNR_2 ligands and indicates that the π_σ frontier orbitals of the PNR_2 ligands interact more strongly than the π^* one. This is due to a better energy match and a larger overlap with the $Ru_4(CO)_{12}$ fragment orbitals in the case of π_σ. Keeping the Ru_4P_2 core arrangement **1** but considering the carbonyl orientation as in Figure 2a changes the local symmetry of the $Ru_4(CO)_{12}$ fragment to D_{2d}, so that now, although planar, the Ru_4 square "sees" two different types of Ru−P bonds. This results in a larger difference between the two computed Ru−P overlap populations, which are 0.400 and 0.345, respectively. Clearly, the carbonyl ligands adapt their positions in order to take into account the nonconical nature of the PNR_2 ligands. Finally, when the core distortion **2** is applied to this latter model, leading to a D_{2d} model as in Figure 2a, the Ru−P overlap populations become equal to 0.631 and 0.134. This model was found to be ≅1.4 eV more stable than the two calculated models based on the planar Ru_4 square of the core framework **1**. On the other hand, when the two PNH_2 ligands are replaced by conical PH phosphinidenes in the model calculations, the core structure **1** is always preferred.

The MO diagram of $Ru_4(CO)_{12}(\mu_4\text{-}PNH_2)_2$ in the D_{2d} idealized geometry of $Ru_4(CO)_{12}(\mu_4\text{-}PNPr^i_2)_2$ (Figure 2a) is shown in Figure 5. The a_1 HOMO is directly derived from the b_{1u} level of clusters of type **1** (Figure 1). The Δ_2 gap is larger than Δ_1. When the core arrangement **1** is imposed on this D_{2d} model, Δ_2 (0.92 eV) becomes smaller than Δ_1 (1.28 eV). Clearly, the core structure **2** favors the actual 64-MVE (8-SEP) count, while the regular arrangement **1** favors the 62-MVE (7-SEP) count. These results are fully consistent with the structure of the known compounds.[2,4] They are essentially due to the fact that the puckering of the M_4 square somewhat lowers the antibonding character of the crucial "b_{1u}" level of Figure 1.

Calculations on the real compounds $Ru_4(CO)_{12}(\mu_4\text{-}PNEt_2)_2$ and $Ru_4(CO)_{12}(\mu_4\text{-}PNPr^i_2)_2$ using their X-ray molecular structures gave results that are very similar to those obtained on the idealized D_{2d} $Ru_4(CO)_{12}(\mu_4\text{-}PNH_2)_2$ model. Finally, it should be noted that in all the calculated $Ru_4(CO)_{12}(\mu_4\text{-}PNH_2)_2$ models some P···P bond-

(11) Kahlal, S.; Saillard, J.-Y.; Hamon, J.-R.; Manzur, C.; Carrillo, D. *J. Chem. Soc., Dalton Trans.* **1998**, 1229.

(12) (a) Adams, R. D.; Babin, J. E.; Estradia, J.; Wang, J.-G.; Hall, M. B.; Low, A. A. *Polyhedron* **1989**, *8*, 1885. (b) Albright, T. A.; Ae Yee, K.; Saillard, J.-Y.; Kahlal, S.; Halet, J.-F.; Leigh, J. S.; Whitmire, K. H. *Inorg. Chem.* **1991**, *30*, 1179. (c) Kahlal, S.; Halet, J.-F.; Saillard, J.-Y. *Inorg. Chem.* **1991**, *34*, 2567. (d) Jun, C. S.; Halet, J.-F.; Rheingold, A. L.; Fehmer, T. P. *Inorg. Chem.* **1995**, *34*, 2101. (e) Carty, A. J.; Hogarth, G.; Enright, G.; Frapper, G. *J. Chem. Soc., Chem. Commun.* **1997**, 1883.

Table 4. Major DFT-Computed Structural and Energetical Data (Averaged Metrical Experimental Data Are Also Given for Comparison)

	$Ru_4(CO)_{12}(PNR_2)_2$ averaged experimental data		$Ru_4(CO)_{12}(PNH_2)_2$		$Ru_4(CO)_{12}(PH)_2$	
	R = Pr^i	R = Et	butterfly	planar	butterfly	planar
relative energy (eV)			0	0.90	0.52	0
HOMO/LUMO gap (eV)			2.09	1.16	1.47	1.11
butterfly angle (deg)	135	137	137	180	158	180
$\Sigma\alpha$(N) (deg)	360	360	360	340		
Ru−Ru (Å)	2.88	2.87	2.93	2.90	2.92	2.86
Ru−P (Å)	2.28; 2.78	2.27; 2.74	2.28; 2.74	2.46	2.35; 2.57	2.44; 2.45
P−N (Å)	1.67	1.66	1.66	1.70		

	Free PNH_2	$[Ru_4(CO)_{12}(PNH_2)_2]^{2+}$		$[Ru_4(CO)_{12}(PH)_2]^{2+}$	
	PNH_2	butterfly	planar	butterfly	planar
relative energy (eV)		0	0.35	0.55	0
HOMO/LUMO gap (eV)		1.38	1.47	1.91	2.08
butterfly angle (deg)		159	180	169	180
$\Sigma\alpha$(N) (deg)	360	360	358		
Ru−Ru (Å)		2.87	2.87	2.91	2.84
Ru−P (Å)		2.38; 2.60	2.48	2.42; 2.54	2.47; 2.47
P−N (Å)	1.65	1.65	1.66		

ing interaction was computed (overlap population ≅ 0.02), as found previously in all the M_4E_2 clusters of type **1**.[1,12]

From the results discussed above, one can simply rationalize the **1** → **2** distortion afforded by the $Ru_4(CO)_{12}(\mu_4\text{-}PNR_2)_2$ clusters by the two canonical formulas **3** and **4**. In **3**, both π-type frontier orbitals of the PNR_2 ligands participate equally in the bonding, while in **4**, only π_σ is involved. The Ru atoms obey the 18-electron rule in both canonical formulas, while P is hypervalent in **3** and satisfies the octet rule in **4**. From this qualitative description of the bonding in $Ru_4(CO)_{12}(\mu_4\text{-}PNR_2)_2$ clusters, one is tempted to predict that, if energetically allowed, the rotational motion on one PNR_2 ligand with respect to the other one does not involve a transition state of pseudo-D_{2d} symmetry in which both PNR_2 units would be coplanar, but rather a structure of type **3** with pseudo-C_{2h} symmetry. Such a geometry in which the nitrogen atoms are pyramidalized would cancel the double-bond character of the PN bond and allow both π-type ligand frontier orbitals to become quasi-equivalent, i.e., would render the PNR_2 fragments conical. To bring a more quantitative overview to this EHT analysis, a series of DFT calculations have been carried out on $Ru_4(CO)_{12}(\mu_4\text{-}PNH_2)_2$ and $Ru_4(CO)_{12}(\mu_4\text{-}PH)_2$ models.

DFT Calculations. The full geometry optimization of $Ru_4(CO)_{12}(\mu_4\text{-}PNH_2)_2$ under the D_{2d} symmetry constraint gives a Ru_4P_2 core of type **2** with a molecular structure such as in Figure 2a. This optimized geometry is in excellent agreement with the experimental molecular structures of $Ru_4(CO)_{12}(\mu_4\text{-}PNR_2)_2$ (R = Pr^i, Et),[4] as shown by the optimized metrical data given in Table 4. It is interesting to note that the computed P−N separation in this model (1.66 Å) is only slightly longer than that optimized for the free PNH_2 ligand (1.65 Å), for which a full double bond is expected.

This optimized geometry was then transformed by averaging and setting equal all of the P−Ru bonds, in such a way that a cluster core of type **1** was then generated. A geometry optimization was then carried out under the only constraint of maintaining a square-planar Ru_4 framework. No symmetry constraint was imposed, to allow the PNR_2 ligands to freely pyramidalize and/or rotate. A geometry of approximate S_4 symmetry was obtained. The major structural parameters are given in Table 4. It is noteworthy that in this structure the P−N bond is longer than in the D_{2d} geometry, and the N atoms are pyramidalized, their hybridization mode being halfway between sp^3 and sp^2. Clearly, the bonding of this close-to-C_{2h} structure is best described by **3**. It is less stable than the D_{2d} ground state by 0.9 eV. Although this geometry optimization is by no means a full search for a transition state, this energy value gives an order of magnitude of the barrier associated with the rotational process that a PNR_2 ligand would undergo.

To compare the bonding properties of a PNR_2 fragment with a conical PR regular phosphinidene ligand, we also carried out full DFT optimization on the $Ru_4(CO)_{12}(\mu_4\text{-}PH)_2$ model, assuming D_{2d} symmetry. In this molecular model, only the local D_{2d} symmetry of the $Ru_4(CO)_{12}$ fragment can create inequivalent P−Ru bonds, i.e., the distorted core **2**. As expected, this core distortion is much weaker (≅50% less pronounced) than in the case of $Ru_4(CO)_{12}(\mu_4\text{-}PNH_2)_2$ (see Table 4). Moreover, this D_{2d} conformation is not the more stable one. The lowest energy of $Ru_4(CO)_{12}(\mu_4\text{-}PH)_2$ was found for a C_{4h} conformation (such as in Figure 2b) for which all the Ru−P bonds are symmetry-equivalent (Table 4). Clearly, the conical PR ligands prefer to bind to a C_{4h} conical $Ru_4(CO)_{12}$ unit.

Four similar DFT geometry optimizations were also carried out on $[Ru_4(CO)_{12}(\mu_4\text{-}PNH_2)_2]^{2+}$ and $[Ru_4(CO)_{12}(\mu_4\text{-}PH)_2]^{2+}$ cations. The major results are reported in Table 4. With two electrons less, i.e., 62 MVEs or 7 SEPs, the preference for the core structure **2** is less pronounced in the case of PNH_2 ligands (by 0.35 eV, vs 0.90 eV in the neutral species). Moreover, the **1** → **2** distortion is reduced by ∼50% as compared to the neutral species. A similar damping is found for the case of the PH ligands in the D_{2d} model. These results confirm that the cluster electron count is in part responsible for the **1** → **2** core distortion observed in the $Ru_4(CO)_{12}(\mu_4\text{-}PNR_2)_2$ clusters.

Conclusion

The cluster core distortion **1** → **2** observed in the molecular structure of the $Ru_4(CO)_{12}(\mu_4\text{-}PNR_2)_2$ compounds, as compared to the other $M_4L_n(\mu_4\text{-}E)_2$ species, originates from several factors: (i) the nonconical nature of the PNR_2 ligands in which some PN double-bond character is always present, rendering its two π-type frontier molecular orbitals (FMOs) inequivalent; (ii) the nonconical nature of the $Ru_4(CO)_{12}$ metallic fragment, induced by the orientation of its CO ligands; (iii) the synergy between the nonconical bonding abilities of the PNR_2 and $Ru_4(CO)_{12}$ moieties, which strengthens the distortion; replacing the PNR_2 ligands by conical PR units would favor a CO orientation, which would make the $Ru_4(CO)_{12}$ fragment conical; (iv) the puckering of the Ru_4 framework in **2,** which tends to stabilize the HOMO of these 64-MVE (8-SEP) compounds, i.e., to favor the $\Delta_2 < \Delta_1$ situation, which is normally disfavored in the case of ruthenium species (see the Introduction section). This additional stabilization would not be present in a 7-SEP species, for which a weaker distortion is expected. Therefore, we conclude that the presence of PNR_2 ligands induces the Ru_4 puckering and in turn favors the 8-SEP count, which is not observed for other $Ru_4(\mu_4\text{-}E)_2$ species.

From this point of view, it is interesting to note that the 8-SEP cluster $Fe_4(CO)_{11}[P(OMe)_3](P\text{-}p\text{-}Tol)_2$ also exhibits pseudo-D_{2d} symmetry illustrated in **2** and the same ligand arrangement as in Figure 2a.[13] However, with a butterfly angle of 163° the core distortion is 2 times less than in the title compounds. This can be attributed to the moderately nonconical nature of the P-*p*-Tol fragment, induced by the conjugation of the aromatic moiety with the phosphorus atom.

Finally it should be noted that, although significant, the inequivalency of the two π-type FMOs of PNR_2 is not very large. In terms of frontier orbitals, PNR_2 is closer to PR than to $(PR_2)^-$. Nevertheless, this ambivalent nature remains to be fully explored. We are currently investigating by DFT calculations the various possible modes of coordination of PNR_2 to transition metals.

Acknowledgment. We thank Dr. J.-F. Halet for helpful discussions. Computing facilities were provided by the Centre de Ressources Informatiques (CRI) of Rennes and the Institut de Développement et de Ressources en Informatique Scientifique du Centre National de la Recherche Scientifique (IDRIS-CNRS). Financial support (to A.J.C.) was provided by the National Research Council of Canada and the Natural Sciences and Engineering Research Council of Canada.

Supporting Information Available: Tables of crystal data, atomic coordinates, thermal parameters, and bond distances and angles for $Ru_4(CO)_{12}(\mu_4\text{-}PNEt_2)_2$. This material is available free of charge via the Internet at http://pubs.acs.org.

OM991038R

(13) Vahrenkamp, H.; Wolters, D. *Organometallics* **1982**, *1*, 874.